

# Preparation of Tumor Hypoxia Sensitive Nanomotors

## Group Member

*Zeyu Wang*

## Instructor

*Dr. Jinzhi Du*

## School

*International Department,  
The Affiliated High School of South China Normal University*

## Location

*Guangzhou, China*

## Table of Contents

Statement of Originality.....	3
List of Figures .....	4
List of Tables .....	5
Abstract.....	6
1. Introduction .....	6
1.1 Janus Particles.....	6
1.2 Preparation Methods of Janus Particles .....	7
1.3 Nano- and Micromotors .....	9
1.4 Tumor Hypoxia and Tumor Penetration .....	10
1.5 Purpose of This Study.....	11
2. Apparatus and Experimental Setup .....	12
2.1 Apparatus .....	12
2.2 Important Experimental Setup .....	12
2.3 Materials .....	14
3. Procedures .....	15
3.1 Synthesis of SiO <sub>2</sub> Nanoparticles .....	15
3.2 Synthesis of SiO <sub>2</sub> Microparticles .....	16
3.3 Preparation of SiO <sub>2</sub> /MnO <sub>2</sub> Janus Nanoparticles by Pickering Emulsion.....	16
3.4 Preparation of Dye-Labeled SiO <sub>2</sub> Janus Microparticles .....	17
3.5 Motion of Janus Particle in H <sub>2</sub> O <sub>2</sub> solution.....	18
3.6 Analysis of the Locomotion of Janus Particle .....	18
4. Results and Discussion .....	19
4.1 Synthesis of SiO <sub>2</sub> Nano- and Microparticles .....	19
4.2 Preparation of SiO <sub>2</sub> /MnO <sub>2</sub> Janus Nanoparticles by Pickering Emulsion.....	22
4.3 Fluorescent Imaging of FITC-Labeled SiO <sub>2</sub> Janus Microparticles.....	24
4.4 Synthesize SiO <sub>2</sub> @MnO <sub>2</sub> Janus Particle .....	25
4.5 Locomotion of SiO <sub>2</sub> @MnO <sub>2</sub> Janus Particle Triggered by H <sub>2</sub> O <sub>2</sub> .....	27
5. Conclusions.....	28
ACKNOWLEDGEMENTS.....	29
References:.....	29

## Statement of Originality

The research process and result of this team are conducted and derived under the guidance of the instructor. Other than the referenced content and the acknowledged sources, this paper does not include any published findings by this group or any other researchers. If there is any inaccuracy, this team is accountable for all the liabilities.

Signature: Zeyu Wang

Date: 9.15.2018

## List of Figures

- 1-1. Different Types of Janus particles.
- 1-2. Schematic procedure to create Janus particles by functionalizing silica particles onto Pickering emulsion of molten paraffin wax and water.
- 1-3. Actuation mechanisms and potential biomedical applications of various types of micro/nanorobots.
- 1-4. The reaction about the acidity-induced, H<sub>2</sub>O<sub>2</sub>-accelerated degradation of MnO<sub>2</sub>.
  - 2.1 Chemical hood in lab.
  - 2.2 Nano Particle Size/Zeta Potential Analyzer in lab.
  - 2.3 JEM-1400 Plus Electron Microscope in University Testing Center.
  - 2.4 JEM-2100 Plus Field Emission Electron Microscope in University Testing Center.
  - 2.5 Inverted Fluorescence Microscope (Olympus) in lab.
- 4.1 Size distribution of silica nanoparticles prepared under different conditions.
- 4.2 TEM images of silica particles of Group A and Group E with hydrodynamic sizes of 141 nm and 633 nm, respectively.
- 4.3 SEM image and DLS measurement of silica microparticles with hydrodynamic size of around 3 μm.
- 4.4 Pictures of the colloidosomes after preparation with Pickering emulsion.
- 4.5 SEM images of the colloidosomes with different formulations under a large field.
- 4.6 SEM images of the colloidosomes with different formulations under a small field.
- 4.7 Fluorescent images of 2 μm silica microparticles with FITC-labelling.
- 4.8 Size distribution and zeta potential of SiO<sub>2</sub> and SiO<sub>2</sub>@MnO<sub>2</sub> Janus nanoparticles.
- 4.9 UV spectra of SiO<sub>2</sub> and SiO<sub>2</sub>@MnO<sub>2</sub> Janus nanoparticles.
- 4.10 a) TEM image of SiO<sub>2</sub>@MnO<sub>2</sub> Janus nanoparticles with silica nanoparticles of 141 nm. b) TEM image of SiO<sub>2</sub>@MnO<sub>2</sub> Janus nanoparticles with silica nanoparticles of 633 nm.
- 4.11 Optical video analysis on nanomotor SiO<sub>2</sub>@MnO<sub>2</sub> Janus nanoparticles.

## List of Tables

1. Information of the materials used in the experiments.
2. Synthesis conditions of SiO<sub>2</sub> Nanoparticle
3. Conditions for the preparation of Pickering emulsion.
4. Size and size distribution of the resultant SiO<sub>2</sub> nanoparticles

## Abstract

In this study, a self-propelled nanomotor based on SiO<sub>2</sub>@MnO<sub>2</sub> Janus nanoparticles was developed. SiO<sub>2</sub> nanoparticles with various diameters were prepared and used as the template. Then, Pickering emulsion using molten paraffin wax and water as oil-water phases was utilized to prepare silica colloidosome, in which the silica nanoparticles was partially embedded in the solidified wax. Then, MnO<sub>2</sub> layer grew on the exposed surface of SiO<sub>2</sub> nanoparticles *via* reducing KMnO<sub>4</sub> aqueous solution. Various measurements including fluorescent imaging, dynamic light scattering (DLS), transmission electronic microscope (TEM), and scanning electronic microscope (SEM) were utilized to characterize the Janus particles. MnO<sub>2</sub> can be degraded under the stimuli of tumor hypoxia environment with high concentration of H<sub>2</sub>O<sub>2</sub> and proton (H<sup>+</sup>) to produce O<sub>2</sub>, so that to propel the locomotion of Janus nanoparticles. Our results indicated that SiO<sub>2</sub>@MnO<sub>2</sub> Janus nanoparticles moved much quicker in 0.5% H<sub>2</sub>O<sub>2</sub> solution in comparison with that in water. This nanomotor strategy might provide new insights to address the long-term issue of limited tumor penetration of cancer nanomedicines.

**Key Words:** Janus particles, nanomotor, tumor hypoxia, H<sub>2</sub>O<sub>2</sub>-responsive, tumor penetration

## 1. Introduction

### 1.1 Janus Particles

Compared to symmetric structures, asymmetry is less favored in production. The everyday objects that people use, such as cars, computers, and books, all more or less displays symmetry rather than asymmetry. However, looking deep inside the human body, many objects, structures, and tissues are highly asymmetric in either chemistry or shape. For example, the asymmetric structure of lipids, having a hydrophilic head

and hydrophobic tails, contribute to their self-organization into bilayers yielding vesicles and size-constraining membranes for cell and bacteria<sup>1</sup>.

Compared with homogenous particles that are commonly prepared and used in the emerging field of nanotechnology, Janus particles are unique objects meeting the features of asymmetry. More importantly, they provide conditions for the coexistence of different chemical and physical properties inside a single particle. Through distinctive biological or chemical methods, scientists have successfully synthesized several identical structures for Janus particles. Figure 1.1 summarized successful particle architectures that have been accomplished so far, including spherical shapes, dumbbell shapes, and vesicle/capsule shapes. The different compartmentalization can be achieved throughout the entire core (core-compartmentalized), or just at the surface by using surface modifiers such as polymers (surface-compartmentalization)<sup>1</sup>.

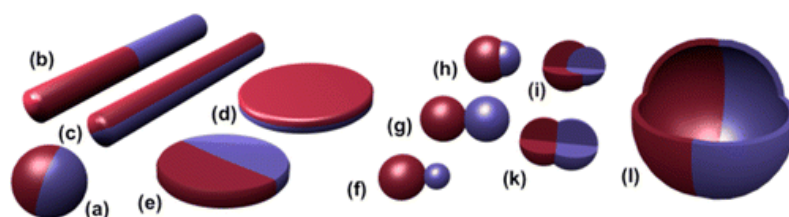


Figure 1.1. Different Types of Janus particles. Spherical (a), two types of cylindrical (b,c), and disc-shaped (d,e) Janus particles. (f–k) Various kinds of dumbbell-shaped JPs with asymmetric or snowman character (f), symmetric appearance (g,k), attached nodes (h), and eccentric encapsulation (i). (l) Janus vesicles or capsules.

## 1.2 Preparation Methods of Janus Particles

Due to the distinct structures and properties of Janus particles, their preparation strategies are markedly different from conventional homogenous particles. Up to date, several methods have been developed for the preparation of Janus particles<sup>1</sup>. One method is to modify homogeneous precursor particles selectively by a mask and release process. A prevailing example is first placing the particles as a monolayer onto planar solid substrates as protecting surfaces. The side that faces the solid substrates is protected from modification, and the other side can be modified by using physical or chemical approaches<sup>2</sup>. This strategy is advantageous for nice control over the surface

area that can be modified, but suffers from the shortcoming that only a few milligrams of particles can be produced in one batch because this approach relies on 2D modification of a monolayer. Microfluidic methods can be used to produce larger quantities, but their particle sizes are limited to 10-100  $\mu\text{m}$  diameter.

Pickering emulsion method can be a prominent strategy of the preparation Janus particles with both great control over the modification areas and in large quantities. Prof Steve Granick from University of Illinois Urbana-Champaign first introduced a unique Pickering emulsion by employing molten paraffin wax and water as the oil-water phases for the production of Janus particles (Figure 1.3)<sup>3</sup>. In their study, silica nanoparticles were chosen as the template, which could be stabilize the emulsion. The emulsion is made at a temperature that higher than the melting point of paraffin wax (usually between 55-65  $^{\circ}\text{C}$ ). After cooling down to room temperature, the wax was solidified and then “locked” the silica particles at frozen wax-aqueous surfaces, preventing particle movement and facilitating subsequent modifications. These emulsions are mechanically and chemically stable, and can be washed and modified by reaction in solution. After surface chemical modification on the aqueous side of the emulsion interface, wax can be dissolved in organic solvent such as chloroform, dichloromethane *etc*, and the resulting particles can be further modified. More interestingly, the embedding distance of silica nanoparticles into the wax, which closely correlates surface area of that can be modified, could be tuned by changing the hydrophobicity of silica nanoparticles using cationic surfactants<sup>4</sup>.

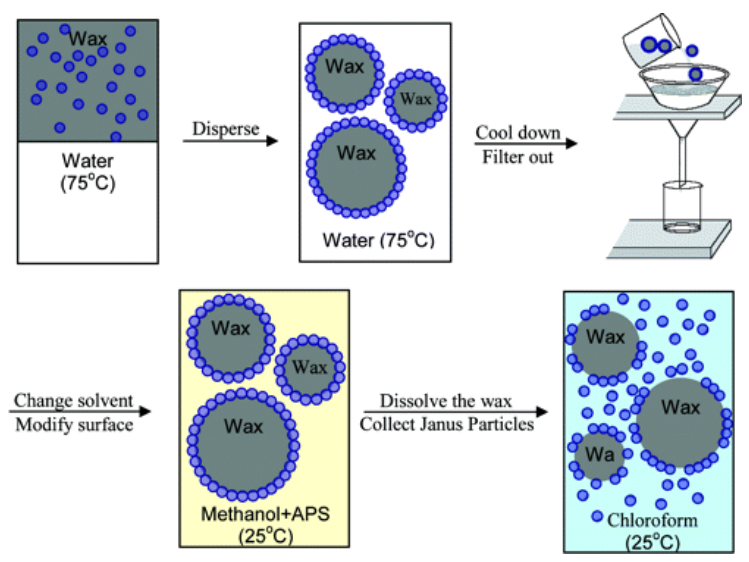


Figure 1.2. Schematic procedure to create Janus particles by functionalizing silica particles onto Pickering emulsion of molten paraffin wax and water. After cooling to room temperature, the colloidosome can be collected by filtering, and the colloidosome can be further modified in solutions for the generation of Janus particles with expected structures and properties. Then, the Janus particles can be obtained after removing wax in organic solvents.

### 1.3 Nano- and Micromotors

Motors and engines are such an important part in human life that hardly anyone can live without the assistance of any possible engine. Not only transportation depends heavily on the use of engines, modern medical science is showing greater interest in the field of using engines as drug loaders, but at a much micro scale. Due to this importance, the three scientists pioneered the study of molecular machines were awarded Noble Prize in 2016. This concept has been further extended to molecular motors, nano- and micromotors, which are fuel-driven or fuel-free motors or engines that can operate on a microscopic scale<sup>5</sup>. Microscopic biological motors and machines are vital components of every living cell and organism. Chemically powered nanomotors in the cell are engaged in protein synthesis, DNA replication, ATP synthesis, cell division and motility.

From a broad context, nanomotors are special Janus particles, with one side capable of generating driving force to enable the motion of particles. Therefore, the methods used to prepare Janus particles can also be employed for the production of nanomotors. Right now, the revolution in nanotechnology has inspired the advances

of nanomotors in medical applications toward improving health care. To meet the requirement for biological applications at these tiny scales, innovative bioinspired design principles are adopted. As shown in Figure 1.2, various types of nano- and micromotors based on distinct actuation principles have been developed. Typically, these tiny machines rely on either chemical stimuli or physical stimuli such as optical, thermal, and electrical energies to drive their motion<sup>6</sup>.

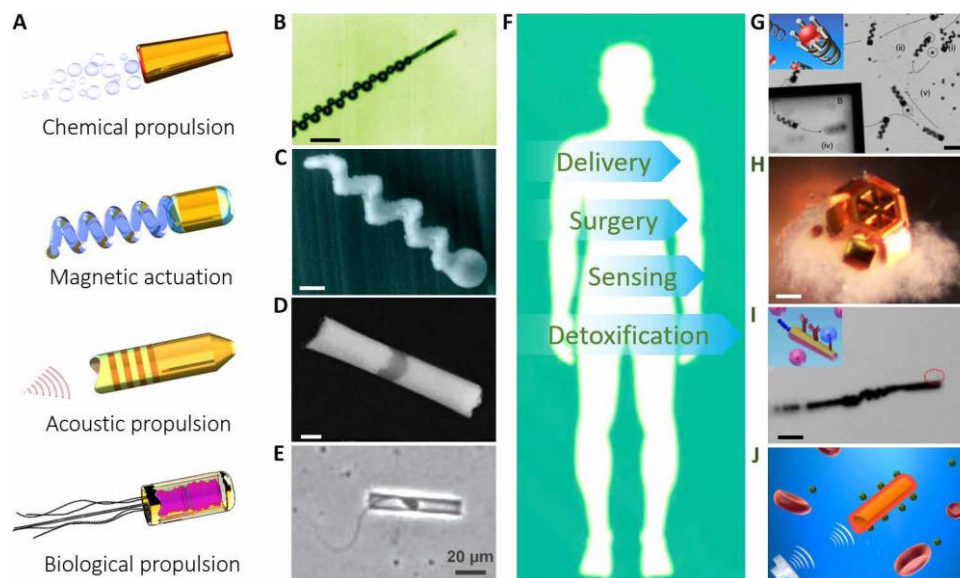


Figure 1.3. Actuation mechanisms and potential biomedical applications of various types of micro/nanorobots. (A) Typical propulsion mechanisms of micro/nanoscale robots. (B) Chemically powered microrocket. (C) Magnetically actuated helical nanoswimmer. (D) Acoustically propelled nanowire motor. (E) Biologically propelled sperm hybrid microrobot. (F) Potential biomedical applications of nanorobots. (G) Magnetic helical microrobot for cargo delivery. (H) Microgrippers for high-precision surgery. (I) Antibody-immobilized microrobot for sensing and isolating cancer cells. (J) RBC membrane-coated nanomotor for biodetoxification.

#### 1.4 Tumor Hypoxia and Tumor Penetration

Tumor hypoxia is a frequently occurred pathological phenomenon, which is the result of a disrupted balance between the supply and consumption of  $O_2$ , due to the abnormal tumor vascular structures in tumors. Hypoxia is a characteristic of the tumor microenvironment, and is reported to be partially responsible for the resistance to radiation therapy, and chemotherapy. More importantly, hypoxia and the high proliferation rate of cancer cells produce excess amounts of reactive oxygen species (ROS), for example, hydrogen peroxide ( $H_2O_2$ )<sup>7</sup>. It has been reported that the  $H_2O_2$

concentration at tumor site is significantly higher than that in normal tissues. Many studies have been performed to use such an endogenous species to design intelligent nanomaterials for improved cancer treatment. A typical example is the use of manganese dioxide (MnO<sub>2</sub>) nanoparticles as the in situ resource of O<sub>2</sub> to modulate tumor hypoxia; due to that MnO<sub>2</sub> nanoparticles show high reactivity and specificity toward H<sub>2</sub>O<sub>2</sub> for the simultaneous and sustained production of O<sub>2</sub> and regulation of pH<sup>8</sup>(Figure 1.4)<sup>7</sup>.

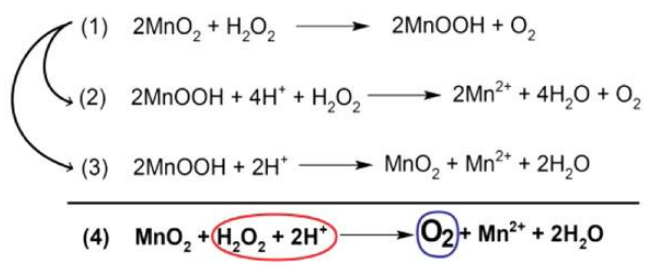


Figure 1.4. The reaction about the acidity-induced, H<sub>2</sub>O<sub>2</sub>-accelerated degradation of MnO<sub>2</sub>.

One more problem caused by the tumor microenvironment is that nanoparticles usually show limited tumor penetration. This has been a long-term bottleneck that limits the efficacy of drug delivery<sup>9</sup>. It is known that solid tumors develop abnormal tumor vasculature and high density of tumor extracellular matrix, and elevated interstitial fluid pressure. Nanoparticles mainly rely on diffusion rather than convection to transport in the tumor interstitial space. The features of the tumor microenvironment imposed dramatic challenges for effective diffusion and distribution of nanoparticles inside tumor tissues. Although several strategies including the design of intelligent nanoparticles have envisioned to overcome this issue<sup>10</sup>, these strategies still rely on the passive diffusion of nanoparticles, which is not sufficient in enhancing particle penetration.

### 1.5 Purpose of This Study

Our study intends to synthesize a tumor hypoxia microenvironment sensitive self-propel nanomotor to enhance tumor site penetration. Our Janus particles function with MnO<sub>2</sub> on one side of the spherical drug loader to provide motion that increases

Brownian motion, which would lead to a deeper penetration after they accumulate at tumor sites. We use the Pickering emulsion method as the main synthesis pathway and utilize several different strategies to create the molecular engine. Potentially this study will have positive therapeutic effects and will be commercially applicable.

## 2. Apparatus and Experimental Setup

### 2.1 Apparatus

BETS-010 Shaking Table (Kylin-Bell Lab Instruments)

DF-101S Heating Plate (Gongyi Yuhua)

RCT Basic Stirrer (IKA)

Analytical Balance Mettler Toledo)

Vortex (IKA)

Ultrasonic Cleaner (Ningbo Scientz)

Glassware (Synthware)

Ultrapure Water (18.2 M, ELGA) Sorvall ST 8R Centrifuge (Thermo Scientific)

Syringe Pump (Baoding Qili)

Nano Particle Size/Zeta Potential Analyzer (Anton Paar GmbH)

Inverted Fluorescence Microscope (Nikon)

JEM-1400Plus Transmission Electron Microscope (TEM, JEOL)

JEM-2100F Field Transmission Electron Microscope (TEM, JEOL)

High Resolution Thermal Field Emission Scanning Electron Microscope (ZEISS Marlin)

### 2.2 Important Experimental Setup

All the experiments related to volatile chemicals were conducted in the well-ventilated chemical hood.



Figure 2.1. Chemical hood in lab.



Figure 2.2. Nano Particle Size/Zeta Potential Analyzer in lab.



Figure 2.3. JEM-1400 Plus Electron Microscope in University Testing Center.



Figure 2.4. JEM-2100 Plus Field Emission Electron Microscope in University Testing Center.

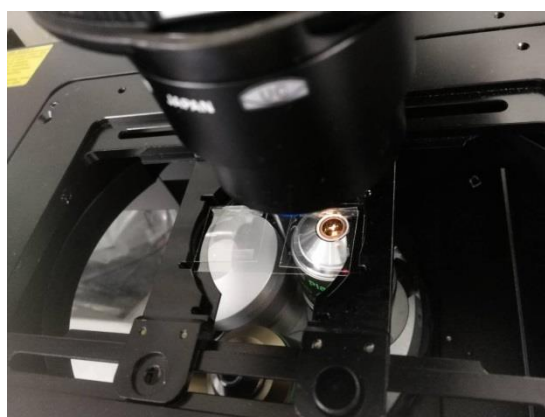


Figure 2.5. Inverted Fluorescence Microscope (Nikon) in lab.

## 2.3 Materials

The detailed information of the materials is listed in Table 1.

Table.1 Information of the materials used in the experiments.

Chemicals	Purity	Vendors
Tetraethyl orthosilicate (TEOS)	>99% (GC)	Aladdin
(3-Aminopropyl)triethoxysilane (APTES)	99%	Aladdin
Ethanol	AR	Sinopharm Chemical Reagent Co.,Ltd
Ammonium hydroxide (NH <sub>4</sub> OH)	AR	Sinopharm Chemical Reagent Co.,Ltd
Potassium permanganate (KMnO <sub>4</sub> )	98%	Guangzhou Chemical Reagent Co.,Ltd

Paraffin	N.A.	Aladdin
Potassium chloride (KCl)	AR	Sinopharm Chemical Reagent Co.,Ltd
Tris(hydroxymethyl) aminomethane hydrochloride (Tris·HCl)	>99%	Aladdin
Didodecyldimethylammonium bromide (DDAB)	98%	Aladdin
Dichloromethane (CH <sub>2</sub> Cl <sub>2</sub> )	AR	Sinopharm Chemical Reagent Co.,Ltd
Hydrogen peroxide (H <sub>2</sub> O <sub>2</sub> )	AR	Guangzhou Chemical Reagent Co.,Ltd
Sulfuric acid (H <sub>2</sub> SO <sub>4</sub> )	AR	Guangzhou Chemical Reagent Co.,Ltd
Fluorescein isothiocyanate (FITC)	≥90% (HPLC)	Sigma-Aldrich

### 3. Procedures

#### 3.1 Synthesis of SiO<sub>2</sub> Nanoparticles

The SiO<sub>2</sub> nanoparticles were prepared by slight modification of Stöber method as described previously<sup>11</sup>. In this method, TEOS were used as the starting material, which was hydrolyzed under the catalysis of NH<sub>4</sub>OH in water/ethanol solution. To get nanoparticles with different sizes, a series of different conditions were tested as shown in the Table 2. Add corresponding amounts of ethanol, ultrapure water, and NH<sub>4</sub>OH solution to a 100 mL round-bottom flask equipped with a magnetic stirrer. The mixed solutions were stirred at 40°C and 650 rpm for 30 min. Then, corresponding TEOS were added to each flask and continued stirring at 40°C overnight. The resulting solution from Group A shows a semi-clear white form. Rest groups were milk white solutions. The solutions were centrifuged at 8500 rpm for 10 minutes in water and ethanol alternately and repeated four times at total. The pellets were vacuum dried for 24 h at 60 °C.

Size and size distribution of the SiO<sub>2</sub> nanoparticles were measured by the Nano Particle Size/Zeta Potential Analyzer. The morphology was characterized by JEM-1400 TEM through dropping an aliquot of the particle solution onto

carbon-coated copper mesh.

Table 2. Synthesis conditions of SiO<sub>2</sub> Nanoparticle

Sample	Ethanol (mL)	Ultrapure water (mL)	NH <sub>4</sub> OH (mL)	TEOS (mL)
Group A	25	0.5	1.7	1.5
Group B	25	0.5	2.5	1.5
Group C	25	0.5	3.4	1.5
Group D	25	0.5	4.2	1.5
Group E	25	0.5	5.0	1.5

### 3.2 Synthesis of SiO<sub>2</sub> Microparticles

SiO<sub>2</sub> microparticles were synthesized using an approach different from that of SiO<sub>2</sub> nanoparticles. First, 0.020 g of potassium chloride in 7 mL water were charged into a round-bottom flask, and then mixed with 60 mL ethanol and 6 mL NH<sub>4</sub>OH. The mixture was kept at 35°C, and termed as solution A. Then, 6.04 mL of TEOS was dissolved in 35 mL ethanol, and termed as solution B. Then, solution B was added to solution A using a syringe pump at the speed of 5.5 mL/h. After completion, the mixture was further stirred at 35 °C at the speed of 350 rpm for 3 h. The solution was centrifuged at 300 rpm for four times to collect the particles. Then, the particles were dried under vacuum.

### 3.3 Preparation of SiO<sub>2</sub>/MnO<sub>2</sub> Janus Nanoparticles by Pickering Emulsion

Pickering emulsion was employed to prepare the Janus particles. Briefly, 10 mg dried SiO<sub>2</sub> nanoparticles (~100 nm) were dissolved in 1.4 mL water and sonicated for a while to dissolve the particles. Various amounts of paraffin wax as indicated in Table 3 were added into the solution in a 10 mL tube with a magnetic stirrer. Sonicated the solution for 30 mins and heated at 80 °C until the wax was completely

molten. Preheated DDAB solution (0.6 mL, 200 mg/L) was added in to the solution. Solidify and filter out the particles, air dry at 25 °C.

Table 3. Conditions for the preparation of Pickering emulsion

Sample	Wax (g)	SiO <sub>2</sub> (mg)	Water (mL)	DDAB Concentration (mg/L)	Total volume (mL)
Group A	0.100	10	1.2	60	2.0
Group B	0.200	10	1.2	60	2.0
Group C	0.300	10	1.2	60	2.0
Group D	0.400	10	1.2	60	2.0
Group E	0.500	10	1.2	60	2.0
Group F	0.600	10	1.2	60	2.0

The obtained particles were dispersed in water, to which 10 mL of 30 mg/mL KMnO<sub>4</sub> solution was added dropwise. The final concentration of KMnO<sub>4</sub> was 20 mg/mL. Place the flask on a mixing rotator and rotate overnight at a speed of 200 rpm. The particles were filtered with water and ethanol until the solution is clear, without any sign of KMnO<sub>4</sub> remaining. The particles were further washed with dichloromethane to remove wax through centrifuging at 8500 rpm and dried under vacuum.

### 3.4 Preparation of Dye-Labeled SiO<sub>2</sub> Janus Microparticles

0.100 g of SiO<sub>2</sub> microparticles was dispensed in 1.6 mL water, to which 0.600 g of wax was added. Sonicate for 30 mins, and heated to 80 °C until the wax was completely melted. Stir at 2600 rpm for five mins and add 0.4 mL DDAB solution (200 mg/L) while stirring. Thirty minutes later, the solution was cooled down to room temperature, and the obtained particles were filtered, washed, and subsequently

dispensed in ethanol containing  $\text{NH}_4\text{OH}$  (aqueous, 25%). After addition of a certain amount of APTES, the mixture was shaken overnight on an orbital shaker at room temperature. The solid was filtered and washed with water. Then, the particles were suspended in water, into which FITC solution was added and shaken for an additional hour. After washing with water for five times, the particles were dissolved in  $\text{CH}_2\text{Cl}_2$ , and centrifuged at 500 rpm to get the FITC-labeled Janus microparticles.

### 3.5 Motion of Janus Particle in $\text{H}_2\text{O}_2$ solution

The motion of the Janus particles was observed by an inverted optical microscopy (Nikon) with  $40\times$  objective lens. Submerge the  $20\times 20$  mm glass coverslip and the  $24\times 50$  mm glass slide in piranha solution ( $\text{H}_2\text{O}_2$  and  $\text{H}_2\text{SO}_4$  with a 1:3 volume ratio) overnight, then use large amount of water to wash the coverslips. After washing with water, wash the slips again with ethanol and dry the glassware. Stick two parallel tapes on the glass slide to provide enough space for the motion of the Janus particles, then drop  $2.5\ \mu\text{L}$  of Janus particle sample in the appropriate concentration onto the slide, and then add  $2.5\ \mu\text{L}$  of  $\text{H}_2\text{O}_2$  solution. Place the smaller coverslip on top of the glass slide. Place the glass slide with the sample under the inverted fluorescence microscope, and then observe locomotion of the particles. Each video of Janus particles was taken by a frame rate about 40 fps with a CCD camera with a frame rate about 60 fps.

### 3.6 Analysis of the Locomotion of Janus Particle

The obtained videos were converted into TIFF sequence images by Adobe After Effects CC 2018 software. The gray of the obtained TIFF sequence images was reversed by the Adobe Photoshop CS4 software and then adjust the exposure of TIFF sequence images to the appropriate value by the same software (batch processing to ensure that each image is processed in the same way). The processed TIFF sequence images was used to analyze the motion of the Janus particle by image J software with Particle Tracker plugin<sup>12</sup> and MATLAB 2017b software with A MATLAB class for Mean Square Displacement analysis<sup>13</sup>. All AVI format video was

converted to MP4 format using the FormatFactory 4.3.0 software.

## 4. Results and Discussion

### 4.1 Synthesis of SiO<sub>2</sub> Nano- and Microparticles

The goal of this study is to construct tumor hypoxia sensitive Janus nano- and micromotors, which can be potentially used as drug delivery systems for enhanced tumor penetration. Inorganic SiO<sub>2</sub> particles are well known for their easy preparation, excellent biocompatibility, and versatile functionality. Therefore, we chose SiO<sub>2</sub> particles as the template for the construction of Janus particles. To control the sizes of SiO<sub>2</sub> particles, different feeding ratios of starting materials, especially the alkali NH<sub>4</sub>OH was changed systemically. After the reaction, the SiO<sub>2</sub> nanoparticles collected by centrifuge. The size and size distribution were measured by dynamic light scattering (DLS) and the results were showed in Table 4, and Figure 4.1. As indicated in Table 4, the particle size was greatly influenced by the amount of NH<sub>4</sub>OH. With NH<sub>4</sub>OH increase, the particle size increased remarkably from 140 nm to 633 nm. More importantly, all the particles were well dispersed in water and had narrow size distributions with polydispersity index (PDI) around 0.1. The results were also confirmed by the DLS profiles in Figure 4.1, from which one could see that all the particles had unimodal size distributions.

Table 4. Size and size distribution of the resultant SiO<sub>2</sub> nanoparticles

Sample	Average Size by Intensity (nm)	Average Size by Number (nm)	PDI
Group A	141.60±3.79	104.80±2.77	0.140
Group B	255.80±8.63	202.10±6.55	0.036
Group C	300.80±18.31	230.80±15.58	0.174
Group D	402.20±14.01	361.50±13.53	0.046
Group E	633.20±15.52	549.80±19.80	0.069

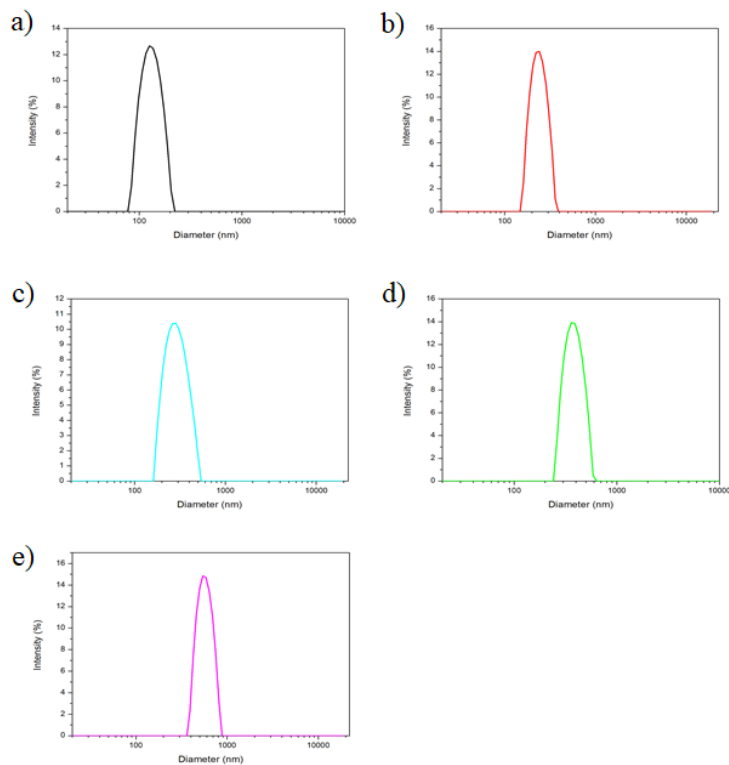


Figure 4.1. Size distribution of silica nanoparticles prepared under different conditions. a-e) correspond to Group A-E in Table 3, in which the amount of added  $\text{NH}_4\text{OH}$  increased from 1.7 to 5.0 mL, respectively.

The typical morphology of silica nanoparticles was verified by TEM observation. As shown in Figure 4.2, the silica nanoparticles of Group A and Group E were well-defined spheres with diameter around 108 and 543 nm, respectively. The nanoparticles were very uniform in size, and well dispersed in water, indicating the synthesis method is very robust. It should also be noted that the average diameter of silica nanoparticles from TEM images is slightly smaller than that obtained from the DLS measurement, which is reasonable since DLS data showed the hydrodynamic diameter in water, while TEM images reflected particles size in dry state.

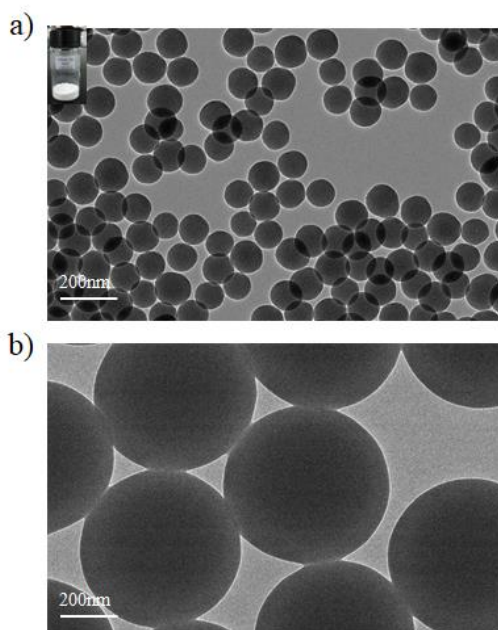


Figure 4.2. TEM images of silica particles of Group A and Group E, respectively.

Besides nanoparticles, silica microparticles could also be made using this method with slight modifications. In this process, the TEOS was added very slowly so that the nucleation process would become very slow, which resulted in particles with larger sizes until several micrometers. To easily observe Janus structure under normal fluorescent microscope, we prepared SiO<sub>2</sub> particles with diameter in micrometer range. In our study, SiO<sub>2</sub> microparticles with average size around 2 μm were obtained. As indicated in Figure 4.3, both the DLS and SEM results confirmed the uniform spherical structures and homogeneous size distribution.

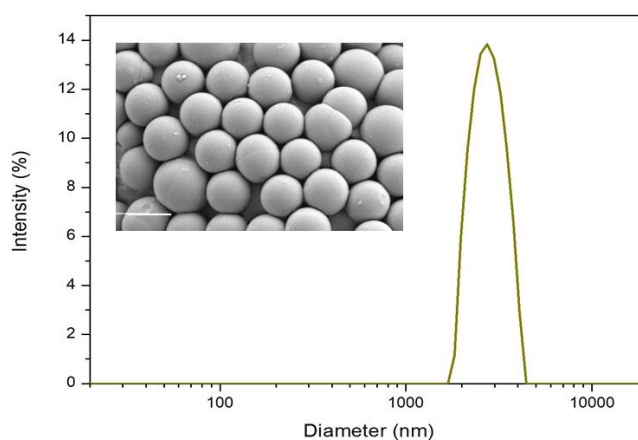


Figure 4.3. SEM image and DLS measurements of silica microparticles. Scale bar is 2 μm.

## 4.2 Preparation of SiO<sub>2</sub>/MnO<sub>2</sub> Janus Nanoparticles by Pickering Emulsion

Several different methods have been reported to prepare Janus particles, among which Pickering emulsion method is a robust one. One prominent advantage of this method is that it allows the preparation of Janus particles in large quantities. In this study, molten wax and water were employed as oil-water phases to prepare Pickering emulsion for the generation of Janus particles. The solidified emulsion was termed as colloidosome. Hydrophobicity of silica particles affects the stability of Pickering emulsion. Pristine SiO<sub>2</sub> nanoparticles are negatively charged, and thus a cationic surfactant DDAB was used to increase the hydrophobicity of SiO<sub>2</sub> nanoparticles to get well packed colloidosome. Our preliminary study verified that the concentration of DDAB at 60 mg/L worked well. Therefore, in current study, we fixed DDAB at 60 mg/L while changing the feed ratio of paraffin to SiO<sub>2</sub> nanoparticles.

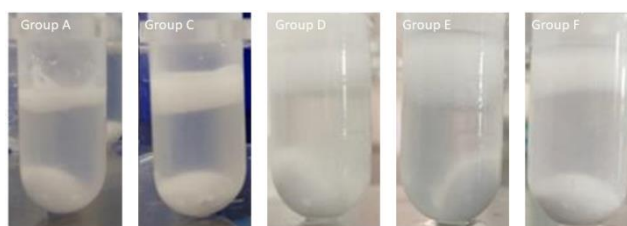


Figure 4.4. Pictures of the colloidosomes after preparation with Pickering emulsion.

The pictures in Figure 4.4 showed the colloidosomes before purification. The white upper layer was the colloidosome because that their overall density might be lower than water. The obtained colloidosomes were characterized by SEM. As shown in Figure 4.5, all the samples formed nearly spherical colloidosome with rough surface and size around 10-15  $\mu\text{m}$ .

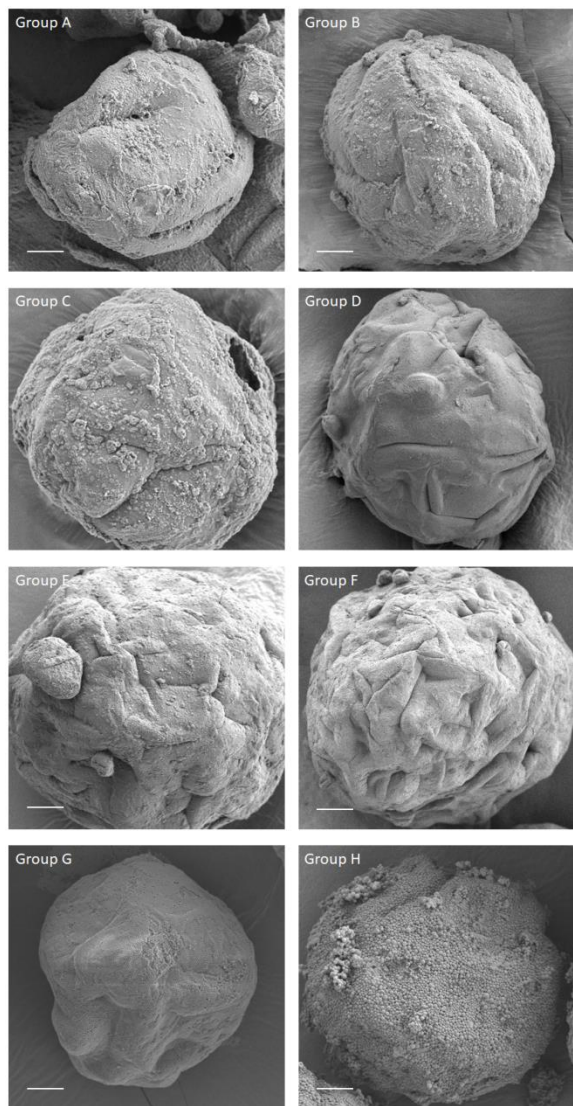


Figure 4.5. SEM images of the colloidosomes with different formulations under a large field. Group A-F correspond to the amount of wax added during preparation is 0.1 g, 0.2 g, 0.3 g, 0.4 g, 0.5 g and 0.6 g with 141 nm silica particles. g) SEM image of wax droplets with 633 nm silica particles. h) SEM image of wax droplets with 2 μm silica particles. Scale bar is 10 μm.

Closely examining the surface of the colloidosome, we can see that different formulations led to different surface packing of SiO<sub>2</sub> nanoparticles. In Group A, B and C with paraffin/particle mass ratios ≤ 30, SiO<sub>2</sub> nanoparticles tended to form large aggregates, and illy packed. Increasing the ratio to ≥ 40, close-packed surface could be achieved (Group D, E, and F), with Group D showing the best nanoparticle packing and minimal aggregation. Group G and H were colloidosomes formed by 633 nm SiO<sub>2</sub> nanoparticles and 2 μm microparticles, both showing well packed silica

structures on the surface.

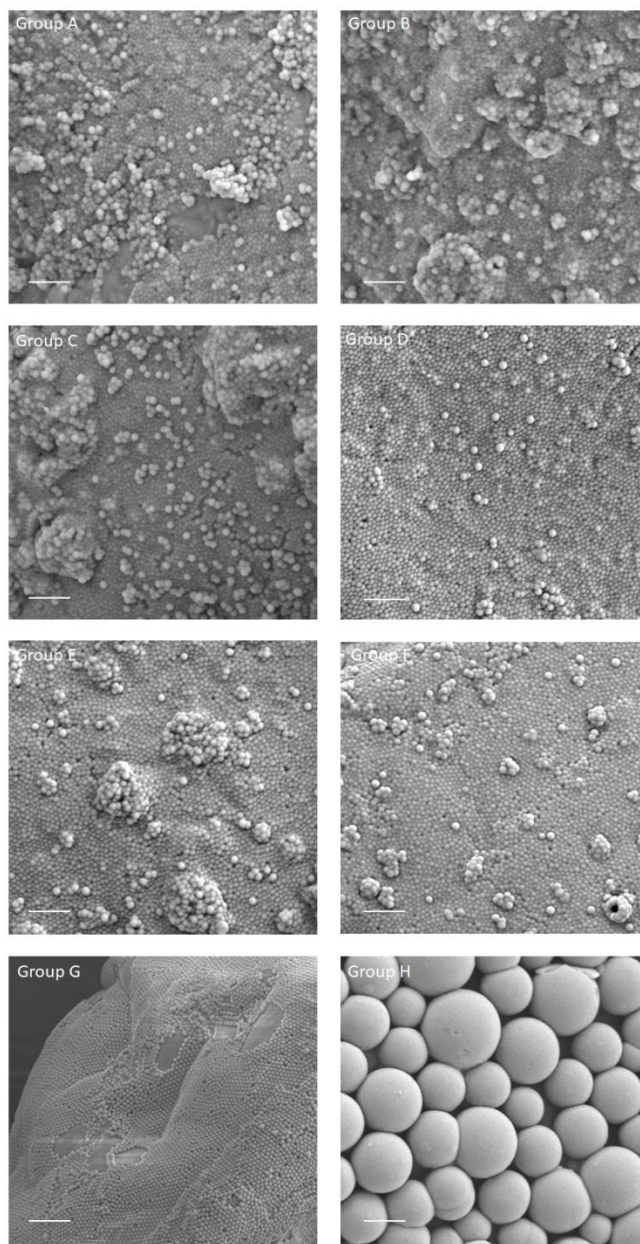


Figure 4.6. SEM images of the colloidosomes with different formulations under a large field. Group A-H correspond to the images in Figure 4.5. Scale bar is 1  $\mu\text{m}$ .

### 4.3 Fluorescent Imaging of FITC-Labeled $\text{SiO}_2$ Janus Microparticles

To visualize the successful construction of the Janus particles by using Pickering emulsion method. We further modified the colloidosome consisting of 2  $\mu\text{m}$   $\text{SiO}_2$  microparticles with a fluorescent dye FITC. One hemisphere of the colloidosome was first modified with APTES to generate amino groups on the surface, and then FITC

was labeled. After release from wax by washing with  $\text{CH}_2\text{Cl}_2$ , the microparticles were observed under inverted fluorescent microscope. As shown in Figure 4.6, the upper panels were particles with homogenous modification with FITC, which displayed uniform fluorescence around the particles. In contrast, the lower panels were Janus particles with half part modifying with FITC, from which we can see that only one side was fluorescent. This result clearly demonstrates that this strategy is applicable in generating Janus particles.

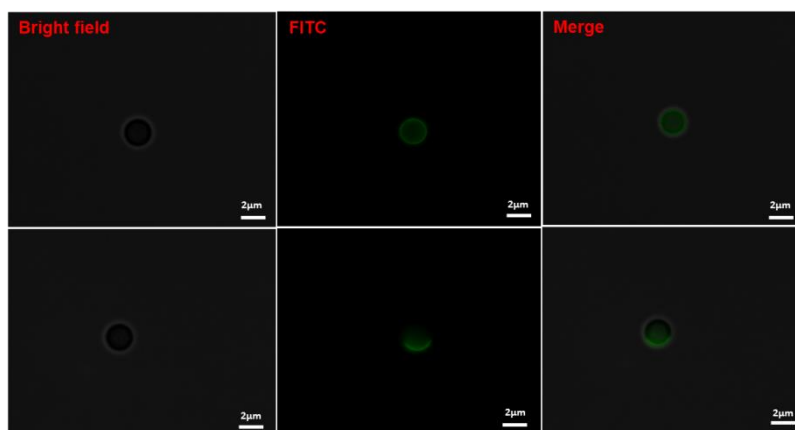


Figure 4.7. Fluorescent images of 2  $\mu\text{m}$  silica microparticles with FITC-labelling. The upper panels are homogeneous particles, while the lower panels are Janus particles.

#### 4.4 Synthesize $\text{SiO}_2@\text{MnO}_2$ Janus Particle

Next, we tried to obtain  $\text{SiO}_2@\text{MnO}_2$  Janus nanoparticles for the purpose of preparing nanomotors. The colloidosome was dispersed in water, and  $\text{KMnO}_4$  was used to produce  $\text{MnO}_2$  on the exposed surface of the colloidosome. As indicate in Figure 4.8, the size was slightly increased due to the deposition of  $\text{MnO}_2$  layer on the surface, while the zeta potential was also increased.

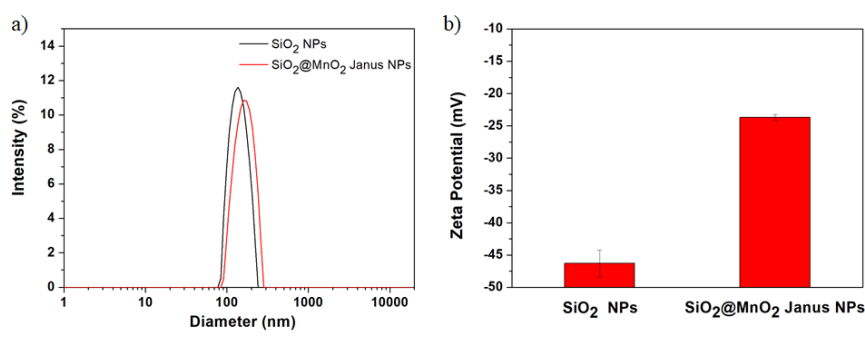


Figure 4.8. Size distribution and zeta potential of SiO<sub>2</sub> and SiO<sub>2</sub>@MnO<sub>2</sub> Janus nanoparticles. Raw silica particles are 141 nm.

The deposition of MnO<sub>2</sub> was also accessed by UV-Vis spectrometer. The raw material of KMnO<sub>4</sub> shows two major absorbance peaks at 320 nm and 540 nm, while pure MnO<sub>2</sub> nanoparticles showed strong absorption between 250-500 nm. Both the SiO<sub>2</sub>@MnO<sub>2</sub> homogenous particles and SiO<sub>2</sub>@MnO<sub>2</sub> Janus particles showed characteristic absorbance of MnO<sub>2</sub>, indicating that SiO<sub>2</sub> nanoparticles could reduce KMnO<sub>4</sub> to MnO<sub>2</sub> without other reducing agents. We propose that the unreacted organosilica existing on the surface of silica nanoparticles might work as the reducing agent.

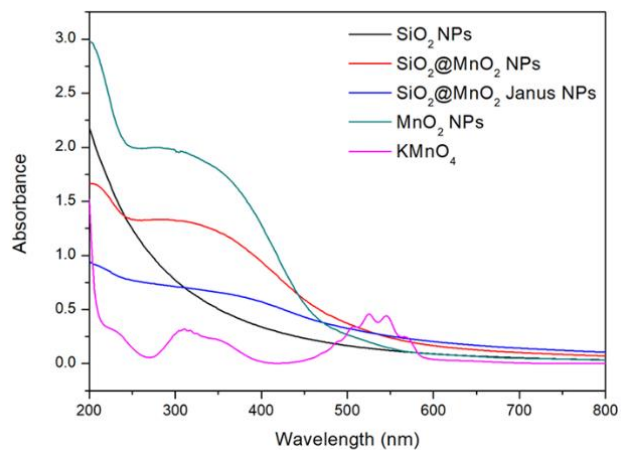


Figure 4.9. UV spectra of SiO<sub>2</sub> and SiO<sub>2</sub>@MnO<sub>2</sub> Janus nanoparticles. Raw silica particles are all 141 nm.

The SiO<sub>2</sub>@MnO<sub>2</sub> Janus particles were further characterized by TEM observations. As indicated in Figure 4.10, both the 141 nm and 633 nm silica

nanoparticles can be used as the template to produce Janus nanoparticles. One can clear see that MnO<sub>2</sub> layer only grew on one side of the particles.

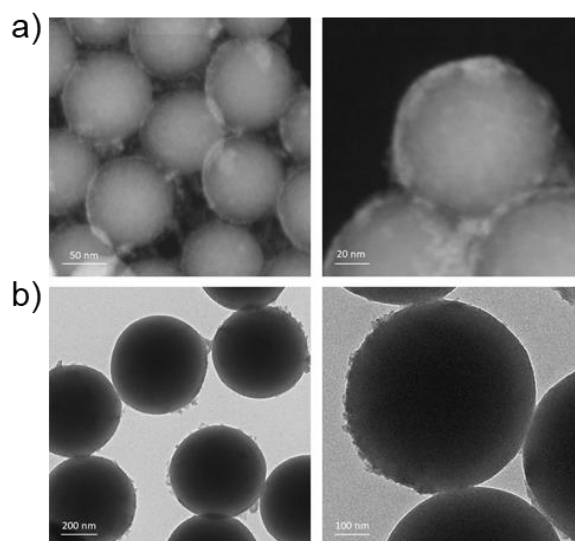


Figure 4.10. a) TEM image of SiO<sub>2</sub>@MnO<sub>2</sub> Janus nanoparticles with silica nanoparticles of 141 nm. b) TEM image of SiO<sub>2</sub>@MnO<sub>2</sub> Janus nanoparticles with silica nanoparticles of 633 nm.

#### 4.5 Locomotion of SiO<sub>2</sub>@MnO<sub>2</sub> Janus Particle Triggered by H<sub>2</sub>O<sub>2</sub>

The mean-square displacement (MSD), are often used to analyze the dynamic motion of particles and is obtained by averaging all the displacements that occurred at a fixed delay  $\Delta t$ . The mean square displacement can be calculated as follows.

$$\langle MSD(\Delta t) \rangle = \langle [x(t + \Delta t) - x(t)]^2 + [y(t + \Delta t) - y(t)]^2 \rangle$$

For the two-dimension motion, the diffusion coefficient (D) is obtained by the following equation<sup>14</sup>.

$$MSD(\Delta t) = 4 \cdot D \cdot \Delta t$$

Based on the two equations, we used the image J software with Particle Tracker Plugin to track the two-dimension motion of Janus particles and obtain the trajectory and the diffusion coefficient of Janus particles. And then we used a MATLAB class msdanalyzer to analyze the Mean Square Displacement.

To confirm the propel motion of the Janus particles, trajectories of the SiO<sub>2</sub>@MnO<sub>2</sub> Janus particles was obtained from the optical videos with and without

H<sub>2</sub>O<sub>2</sub> as shown in Figure 4.11. With adding of H<sub>2</sub>O<sub>2</sub>, the trajectory of SiO<sub>2</sub>@MnO<sub>2</sub> Janus particles was longer and more directionally than the Janus particles in the pure water. Compared to Brownian motion, the diffusion coefficient of SiO<sub>2</sub>@MnO<sub>2</sub> Janus particles was enhanced from about 0.56 μm<sup>2</sup>/s to 1.26 μm<sup>2</sup>/s, which was increased by 2.25 times. As indicated in Figure 4.11, the MSD of SiO<sub>2</sub>@MnO<sub>2</sub> Janus particles in H<sub>2</sub>O<sub>2</sub> solution was clearly much longer than the SiO<sub>2</sub>@MnO<sub>2</sub> Janus particles in water, which can confirm the self-propel motion of the Janus particles.

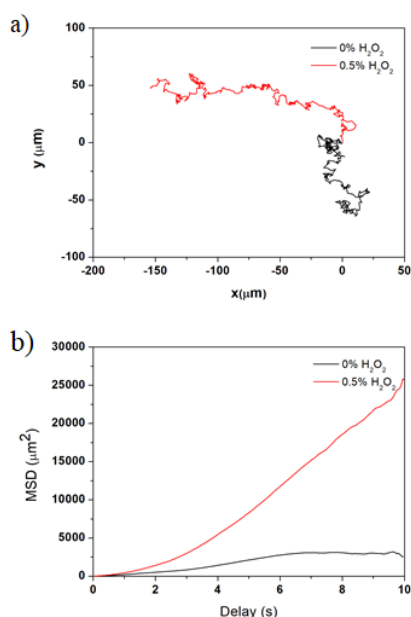


Figure 4.11. Optical video analysis on nanomotor SiO<sub>2</sub>@MnO<sub>2</sub> Janus nanoparticles. a) Trajectory tracking of the SiO<sub>2</sub>@MnO<sub>2</sub> NPs with different H<sub>2</sub>O<sub>2</sub> concentrations up to 10 s. b) Plot of mean square displacement (MSD) versus time delay (s), analyzed from the trajectory tracking in a).

## 5. Conclusions

In this study, we constructed SiO<sub>2</sub>@MnO<sub>2</sub> Janus particles as nanomotors for potential application as drug delivery systems. Various measurements including fluorescent imaging, DLS, TEM, and SEM were utilized to characterize the Janus structure, which all proved the success in producing Janus particles *via* the Pickering emulsion method. MnO<sub>2</sub> was chosen to generate the Janus structure due to its responsiveness to tumor hypoxia environment with high concentration of H<sub>2</sub>O<sub>2</sub> and proton (H<sup>+</sup>). Under the stimuli of H<sub>2</sub>O<sub>2</sub> and H<sup>+</sup>, the MnO<sub>2</sub> can be degraded to produce O<sub>2</sub>, so that to propel the locomotion of nanoparticles in the tumor matrix to potentially

address the long-term issue of limited tumor penetration of cancer nanomedicines. It should also be noted that the nanometers presented in current work only demonstrates the feasibility of this concept in enhancing the movement of nanoparticles, more biological evaluations are still needed for future applications as a powerful drug delivery system.

## ACKNOWLEDGEMENTS

Great thanks to Dr Jinzhi Du and Miss Qiuyue Huang in Smart Nanomedicine Lab for their guidance and help during my project. Thanks for the help of Mrs Jie Cui, Mrs Xiaodong Wu, Mr Ji Yang at South China University of Technology for their help in TEM and SEM measurements.

## References:

1. Walther, A.; Müller, A. H. E., Janus Particles: Synthesis, Self-Assembly, Physical Properties, and Applications. *Chemical Reviews* **2013**, *113* (7), 5194-5261.
2. Lee, T. C.; Alarcóncorrea, M.; Miksch, C.; Hahn, K.; Gibbs, J. G.; Fischer, P., Self-Propelling Nanomotors in the Presence of Strong Brownian Forces. *Nano Letters* **2015**, *14* (5), 2407.
3. Hong, L.; Jiang, S.; Granick, S., Simple method to produce Janus colloidal particles in large quantity. *Langmuir* **2006**, *22* (23), 9495-9499.
4. and, S. J.; Granick, S., Controlling the Geometry (Janus Balance) of Amphiphilic Colloidal Particles. *Langmuir the Acs Journal of Surfaces & Colloids* **2008**, *24* (6), 2438-45.
5. Wang, J.; Gao, W., Nano/Microscale motors: biomedical opportunities and challenges. *Acs Nano* **2012**, *6* (7), 5745-5751.
6. Li, J.; Gao, W.; Zhang, L.; Wang, J., Micro/nanorobots for biomedicine: Delivery, surgery, sensing, and detoxification. **2017**, *2* (4).
7. Prasad, P.; Gordijo, C. R.; Abbasi, A. Z.; Maeda, A.; Ip, A.; Rauth, A. M.; Dacosta, R. S.; Wu, X. Y., Correction to Multifunctional Albumin–MnO<sub>2</sub>Nanoparticles Modulate Solid Tumor Microenvironment by Attenuating Hypoxia, Acidosis, Vascular Endothelial Growth Factor and Enhance Radiation Response. *Acs Nano* **2014**, *8* (6), 3202-3212.

8. Yang, G.; Xu, L.; Chao, Y.; Xu, J.; Sun, X.; Wu, Y.; Peng, R.; Liu, Z., Hollow MnO<sub>2</sub> as a tumor-microenvironment-responsive biodegradable nano-platform for combination therapy favoring antitumor immune responses. *Nature Communications* **2017**, *8* (1), 902.
9. Zhang, Y. R.; Lin, R.; Li, H. J.; He, W. L.; Du, J. Z.; Wang, J., Strategies to improve tumor penetration of nanomedicines through nanoparticle design. *Wiley Interdisciplinary Reviews Nanomedicine & Nanobiotechnology* **2018**, e1519.
10. Li, H. J.; Du, J. Z.; Du, X. J.; Xu, C. F.; Sun, C. Y.; Wang, H. X.; Cao, Z. T.; Yang, X. Z.; Zhu, Y. H.; Nie, S., Stimuli-responsive clustered nanoparticles for improved tumor penetration and therapeutic efficacy. *Proceedings of the National Academy of Sciences of the United States of America* **2016**, *113* (15), 4164.
11. Tang, L.; Fan, T. M.; Borst, L. B.; Cheng, J., Synthesis and Biological Response of Size-Specific, Monodisperse Drug-Silica Nanoconjugates. *Acs Nano* **2012**, *6* (5), 3954-3966.
12. Sbalzarini, I. F.; Koumoutsakos, P., Feature point tracking and trajectory analysis for video imaging in cell biology. *Journal of Structural Biology* **2005**, *151* (2), 182-195.
13. Tarantino, N.; Tinevez, J. Y.; Crowell, E. F.; Boisson, B.; Henriques, R.; Mhlanga, M.; Agou, F.; Israël, A.; Laplantine, E., TNF and IL-1 exhibit distinct ubiquitin requirements for inducing NEMO–IKK supramolecular structures. *Journal of Cell Biology* **2014**, *204* (2), 231-45.
14. Ma, X.; Jannasch, A.; Albrecht, U. R.; Hahn, K.; Miguellópez, A.; Schäffer, E.; Sánchez, S., Enzyme-Powered Hollow Mesoporous Janus Nanomotors. *Nano Letters* **2015**, *15* (10), 7043.